Climate Dynamics (2021) 57:2687–2700
https://doi.org/10.1007/s00382-021-05830-9

Pacific circulation response to eastern Arctic sea ice reduction in seasonal forecast simulations

Anne Seidenglanz[1] · Panos Athanasiadis[1] · Paolo Ruggieri[1,2] · Ivana Cvijanovic[3] · Camille Li[4,5] · Silvio Gualdi[1,6]

Received: 17 November 2020 / Accepted: 27 May 2021 / Published online: 22 June 2021

Abstract
Recent studies point to the sensitivity of mid-latitude winter climate to Arctic sea ice variability. However, there remain contradictory results in terms of character and timing of Northern Hemisphere large-scale circulation features to Arctic sea ice changes. This study assesses the impact of realistic late autumn eastern Arctic sea ice anomalies on atmospheric wintertime circulation at mid-latitudes, pointing to a hidden potential for seasonal predictability. Using a dynamical seasonal prediction system, an ensemble of seasonal forecast simulations of 23 historical winter seasons is run with reduced November sea ice cover in the Barents-Kara Seas, and is compared to the respective control seasonal hindcast simulations set. A non energy-conserving approach is adopted for achieving the desired sea ice loss, with artificial heat being added conditionally to the ocean surface heat fluxes so as to inhibit the formation of sea ice during November. Our results point to a robust atmospheric circulation response in the North Pacific sector, similar to previous findings on the multidecadal timescale. Specifically, an anticyclonic anomaly at upper and lower levels is identified over the eastern midlatitude North Pacific, leading to dry conditions over the North American southwest coast. The responses are related to a re-organization (weakening) of west-Pacific tropical convection and interactions with the tropical Hadley circulation. A possible interaction of the poleward-shifted Pacific eddy-driven jet stream and the Hadley cell is discussed. The winter circulation response in the Euro-Atlantic sector is ephemeral in character and statistically significant in January only, corroborating previous findings of an intermittent and non-stationary Arctic sea ice-NAO link during boreal winter. These results aid our understanding of the seasonal impacts of reduced eastern Arctic sea ice on the midlatitude atmospheric circulation with implications for seasonal predictability in wintertime.

Keywords Arctic sea ice · Seasonal prediction · Atmospheric circulation · Tropical Pacific convection · Rossby wave train · Hadley cell-jet interaction

1 Introduction

The Arctic region (60° N–90° N) has undergone profound changes during the past decades, one of which is the near-surface accelerated warming with respect to the global average warming (IPCC report 2019). Diminishing Arctic sea ice cover is ascribed a central role in shaping this "Arctic amplification", while the exact role of this loss in shaping mid-latitude winter climate remains hotly debated. Sea ice loss is apparent in all seasons, with most wintertime loss occurring in the Barents Sea (March, 27%) and most summertime loss occurring in the East Siberian Sea (September, 22%) (Onarheim et al. 2018). Even though pan-Arctic sea ice loss is most pronounced during summer, from a seasonal prediction perspective, November is particularly interesting because Barents-Kara sea ice conditions at this time have

✉ Anne Seidenglanz
annework985@gmail.com; annesa5891@gmail.com

1 Centro Euro-Mediterraneo sui Cambiamenti Climatici (CMCC), Bologna, Italy

2 Dipartimento di Fisica e Astronomia, Università di Bologna, Bologna, Italy

3 Barcelona Supercomputing Center, Centro Nacional de Supercomputatión (BSC-CNS), Barcelona, Spain

4 Geophysical Institute, University of Bergen, Bergen, Norway

5 Bjerknes Centre for Climate Research, Bergen, Norway

6 Istituto Nazionale di Geofisica e Vulcanologia (INGV), Bologna, Italy

been shown to be a source of predictive skill for European winter climate (Koenigk et al. 2016; Scaife et al. 2014). Whether there are implications for the rest of the Northern Hemisphere is less known.

Boreal winter is the time of the year when the climatological turbulent heat fluxes at high latitudes are strongest due to the large temperature difference between the warm ocean and cold atmosphere.

In the Barents-Kara Seas (BKS) sector, November has been identified as the critical month of sea ice forcing of the winter atmospheric circulation due to maxima in both variability and trend of surface heat fluxes. Yet, any larger-scale atmospheric impacts may be delayed by several months (e.g. Deser et al. 2010).

Most research so far has focused on remote signals to observed or projected BKS sea ice variability. Circulation changes in response to autumn BKS sea ice variability have been detected in the Euro-Atlantic sector and Eurasia, including the position and intensity of the jet stream, the associated storm tracks (Seierstad and Bader 2009), transient eddy feedbacks propagating atmospheric circulation anomalies to mid-latitudes (Deser et al. 2004, 2007), as well as a "stratospheric bridge" via constructive wave interference with the climatological stationary wave pattern and a resulting weakening of the stratospheric polar vortex with subsequent downward coupling with the tropospheric North Atlantic Oscillation (NAO) (Peings and Magnusdottir, 2014; Kim et al. 2014; Sun et al. 2020; Nakamura et al. 2015; Ruggieri et al. 2017). Most of these circulation changes have been associated with the negative phase of the NAO settling in late winter, following BKS sea ice reduction in late autumn, a result also found in observational studies (Yang et al. 2016; Nakamura et al. 2015; García-Serrano et al. 2015). Similarly, recently observed harsh winters over northern and central Eurasia have been related to sea ice loss and associated warming in the eastern Arctic, amongst other via increased frequency of atmospheric blocking over the Ural region (Screen and Simmonds 2013; Liu et al. 2012). This pattern is referred to as the "warm Arctic cold continents (WACC)" pattern (Kug et al. 2015).

Most of these studies focused on interannual variability to longer-term trends, and their findings remain inconclusive in terms of the favoured NAO phase and the strength of the signal on these timescales. Recent observational studies, for example, show an intermittent (Siew et al. 2020) and non-stationary (Kolstad and Screen 2019) sea ice-NAO link during winter, while other studies point to a positive NAO-like response (Singarayer et al. 2006; Orsolini et al. 2012), opposing the negative NAO-like circulation response described above. Furthermore, atmospheric responses to sea ice perturbations are subject to large internal variability (e.g. Screen et al. 2013). More recent considerations of the winter Arctic–mid-latitude links doubt the role of Arctic sea ice loss in shaping mid-latitude winter weather and rather suggest anomalous mid-latitude flow might cause both mild Arctic conditions (thus sea ice loss) and cold mid-latitude winters (Blackport et al. 2019; McCusker et al. 2016).

For the longer-term perspective, the atmospheric response to sea ice variability is sensitive to where exactly sea ice is perturbed; pan-Arctic sea ice loss being different from regional sea ice loss (Sun et al. 2020; Screen 2017). Pan-Arctic sea ice loss on the decadal time scale has been shown to trigger circulation changes also in the Pacific sector, and more specifically, has led to ridging at upper and lower levels in the northeast Pacific which resulted in dry conditions over California (Sewall and Sloan 2004; Cvijanovic et al. 2017; Simon et al. 2021).

Here, we demonstrate for the first time that autumn sea ice loss in the eastern Arctic leads to a significant and robust winter circulation response in the Pacific sector on the seasonal timescale. To our knowledge, no study has previously focused on the role of autumn BKS sea ice variability in shaping atmospheric winter circulation in a seasonal prediction framework. One previous study has investigated the transient coupled ocean–atmosphere response to pan-Arctic sea ice thinning in 1-year long simulations (Semmler et al. 2016). However, the focus was on the summer season and adopting pan-Arctic sea ice loss. Here, using a seasonal prediction system, we assess the transient winter atmospheric circulation response to autumn BKS sea ice reduction in a seasonal hindcast framework. An assessment of the transient seasonal circulation response to Arctic sea ice reduction allows assessing the potential for seasonal predictability of wintertime circulation originating from Arctic sea ice anomalies, which is rather different than the forced response that may develop over a number of years. We consider 23 recent winter seasons (1993–2015), so as to take into account different background climate states of different years. The sensitivity experiments are assessed in comparison to an undisturbed "control" ensemble hindcast data set for the same period and initial conditions. A number of realizations (10) per winter season helps to increase the signal-to-noise ratio. We find that sea ice reduction in the BKS leads to a robust circulation response primarily in the northeast Pacific sector.

We begin by describing the model, the experimental setup and the heat flux adjustment method for perturbing November sea ice in Sect. 2. Features of the winter mean circulation response as well as the seasonal evolution of the response are detailed in Sect. 3 with a particular focus on the Pacific sector circulation response. The implications of the results are discussed in Sect. 4.

2 Methods

2.1 Model and data set

The atmospheric circulation response to Arctic sea ice loss is assessed using the seasonal prediction system CMCC-SPSv3 (Euro-Mediterranean Center for Climate Change (CMCC) Seasonal Prediction System version 3) which is used by the Euro-Mediterranean Center for Climate Change in operational mode to issue seasonal forecasts (Sanna et al. 2017). The atmospheric component is the Community Atmosphere Model version 5.3 (CAM 5.3) in a spectral element configuration with a horizontal resolution of about 1° and 46° vertical levels. The model top is at 0.3 hPa which allows the representation of some key stratospheric processes. The ocean model component is the Nucleus for European Modelling of the Ocean 3.4 (NEMO 3.4), sea ice is represented by Community Ice CodE 4 (CICE4), and both have a horizontal resolution of 1/4° and 50 levels. Land/vegetation and river routing are represented by CLM4.5 (Community Land Model version 4.5) and the RTM (River Transport Model), respectively. Further details about the initialization strategy, ensemble generation, and other technical details of CMCC-SPSv3 can be found in Sanna et al. (2017).

To assess the atmospheric response to reduced late autumn sea ice cover, we run a set of seasonal ensemble forecasts with perturbed sea ice cover in the BKS during November ("ICEFREE"). These simulations are performed for 23 winter seasons (1993–2015), initialized on November 1 as an ensemble of 10 realizations per season, summing to a total of 230 seasonal simulations (see Table 1 for details).

Details on the procedure to achieve reduced sea ice conditions in November are outlined in Sect. 2.2. These ICEFREE simulations are contrasted with the unperturbed seasonal hindcast data set ("CTRL") over the same time period (1993–2015), with each realization having the same start date (1st November) and identical initial conditions as in ICEFREE. The response to reduced November sea ice concentration is defined as the ensemble mean difference between the perturbed (ICEFREE) and unperturbed (CTRL) climates (ICEFREE minus CTRL). The statistical significance of the response to sea ice reduction is evaluated using a test for differences of the mean for paired samples (Wilks, 2011; see Supplementary Material Sect. 2).

2.2 Sea ice perturbation in ICEFREE

Sea ice cover in the BKS is reduced based on a heat flux formulation that alters SST by adding a feedback term to the non-solar heat fluxes at the ocean surface. This restoring strategy is based on a protocol used for decadal idealized and pacemaker experiments (Boer et al. 2016). The correction to the non-solar heat fluxes (longwave, sensible and latent heat fluxes) is computed in the following way:

$$Q_{ns} = Q^0_{ns} + \begin{cases} \frac{dQ}{dT}\left(T|_{k=1} - SST_{Target}\right) & if\ T|_{k=1} \leq -1.5^{\circ}C \\ 0\ else \end{cases}$$

Q_{ns} is the corrected sum of the non-solar surface heat fluxes, Q^0_{ns} is the initial uncorrected sum of non-solar heat flux terms, dQ/dT is a fixed, negative feedback coefficient (–5000 $Wm^{-2}\,K^{-1}$) that acts on SST, and $T|_{k=1}$ is the model's temperature at the top layer of the ocean model (effectively SST). SST_{Target} is the target SST towards which the model SST's are nudged at each model time step. Hence, prior to the calculation of Q_{ns}, additional heat flux is applied as a correction to $T|_{k=1}$. The restoring is active on a conditional basis, meaning that it is active only when SST drops below – 1.5 °C. The target value is set to SST_{Target} = – 1.6 °C so as to just prevent seawater with a salinity of about 35 psu from freezing. In addition, the SST restoring is active on a regional basis covering the BKS, as depicted by the mask in Fig. 1a. The outer edges form a sponge zone which acts to inhibit steps in SST gradients. Outside of the restoring region, the coupled model evolves freely, allowing for a realistic climate response. The restoring coefficient of – 5000 $Wm^{-2}\,K^{-1}$ that determines (yet not alone) the amount of heat added to the upper ocean is chosen to be a large value so as to make the nudging effective, being aware of the very small temperature difference between SST_{Target} and the restoring activation temperature (– 1.5 °C). The default heat added used for multi-decadal pacemaker experiments (–40 $Wm^{-2}\,K^{-1}$; Boer et al. 2016) did not achieve the desired change in sea ice cover over the timescale of interest and is thus unsuitable for the purpose of this experiment. Please

Table 1 Experimental set-up adopted in this study

Characteristic	ICEFREE	CTRL
Hindcast period	1993–2015 (23 winter seasons)	1993–2015 (23 winter seasons)
Realizations per winter season	10	10
Start date	1st November	1st November
Simulation length	6 months (1st Nov–30th April)	6 months (1st Nov–30th April)
November ice sea perturbation	Heat supply to the upper ocean layer	None

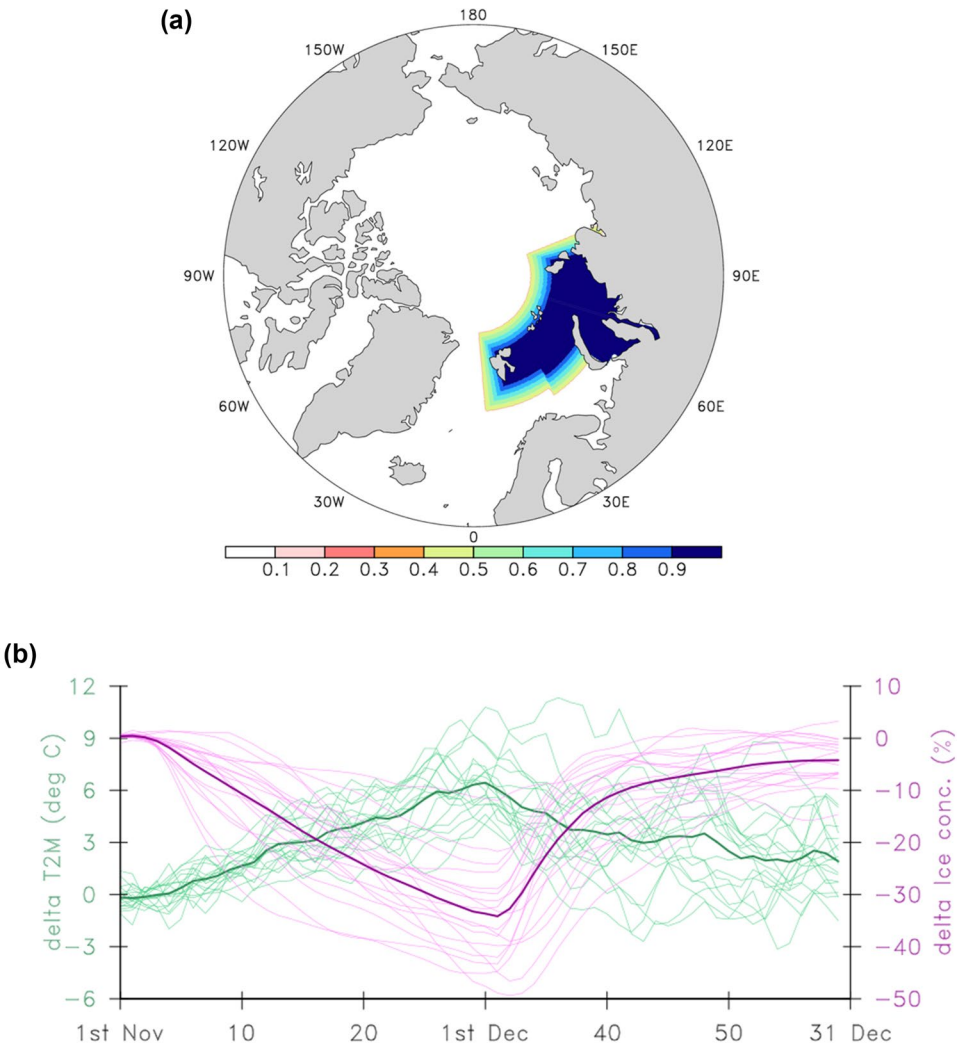

Fig. 1 **a** Mask indicating the region where restoring on SSTs is active (covering the north of the Barents Sea and entire Kara Sea). Values of zero indicate that the restoring is never activated in that region; values equal to 1 indicate that the restoring is fully active (coefficient of 1.0). Values in-between vary correspondingly. **b** Time series of difference in near-surface temperature (T2M, green lines) and in sea ice concentration (SIC, purple lines) area-averaged over the BKS (25–90° E, 75–80° N) during the first two months of the integration (November and December). Faint lines represent the means of single years in the period 1993–2015, the thick lines represent the ensemble mean differences

note that additional heating of the atmosphere is minimal due to the small window within which the heating is active (between – 1.5 °C and about – 1.65 °C when sea water with salinity of 35 psu freezes). The nudging in effect represents a non energy-conserving method for controlling sea ice concentration.

The amount of heat ultimately added to the upper ocean layer during November depends on the amount of sea ice that is already present at the time of initialization, leading to different amounts of sea ice removal in the BKS during each year (Figs. 1b, S.1). Another reason for these differences from year to year is the varying atmospheric circulation (air temperature, wind speed and humidity) above the ocean surface. The ensemble mean of BKS sea ice concentration decreases through November (thick purple line in Fig. 1b), concurrent with an increase in near-surface temperatures (thick green line in Fig. 1b) averaged over the same area. After the nudging is switched off at the end of November, the model evolves freely and sea ice gradually returns to near its climatological value by the end of December, with the associated near-surface air temperature anomalies disappearing.

One of the objectives of our study is to evaluate the atmospheric circulation response to realistic sea ice concentration (SIC) anomalies compatible with the observed sea ice variations in the same period. The CTRL November mean sea ice concentration compares well to the corresponding observed climatology of November mean SIC (Fig. 2c, d). The perturbed November sea ice conditions in ICEFREE also compare well to a composite of sea ice minimum years from reanalysis data (Figs. 2a, b, S2). Consequently, sea ice anomalies arising from the ensemble mean difference (ICEFREE-CTRL) compare well with realistic sea ice anomalies taken from reanalysis data (ERA-Interim) and have a similar spatial structure and magnitude. The lack of anomalous sea ice cover near the coast of Siberia in reanalysis (Fig. 2f) compared to ICEFREE can be explained by the low interannual variability in this area due to shallow waters near the coast, leading to unconditional sea ice formation (hence low variability) during November.

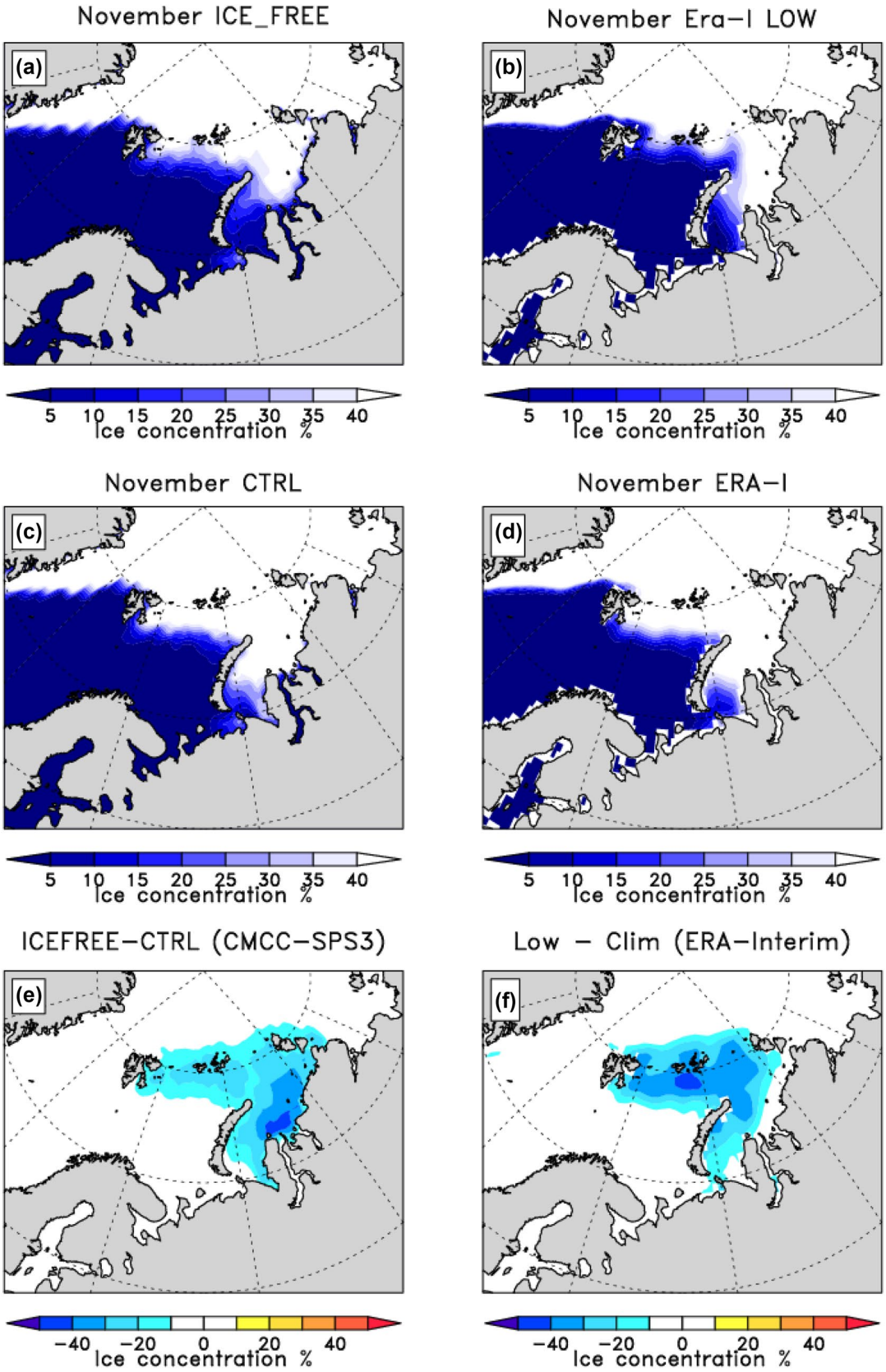

Fig. 2 November mean sea ice concentration (SIC) in **a** the ensemble mean of ICEFREE, **b** in a composite mean of low sea ice years (2000, 2009 and 2012) from reanalysis data (ERA-Interim), **c** in the CTRL model run, and **d** climatological November SIC from ERA-Interim (1993–2015), **e** ICEFREE minus CTRL in the model and **f** low minus climatology in ERA-Interim

3 Results

3.1 Large-scale features of the winter mean response

Figure 3 reveals the winter (DJF) mean response in ICEFREE to the sea ice reduction in late fall. The imposed heat flux and consequent sea ice removal (Fig. 2e) result in a pronounced (> 5 °C) localized, near-surface warming in the BKS (Fig. 3a). There is a heterogeneous surface temperature signal covering the Northern Hemisphere, with surface warming over central and western Europe and a cold anomaly over North America. As will be shown later, in contrast to the ephemeral warming and related circulation response over Europe, the circulation response in the Pacific sector lasts over the entire winter season (Figs. 4, 5).

The mean sea level pressure anomalies indicate a weak positive NAO-like circulation response over the Euro-Atlantic sector, although this response is statistically significant in January only (Fig. 5). This circulation pattern stands in contrast with the negative NAO circulation response to eastern Arctic sea ice loss identified in a number of (Peings and Magnusdottir 2014; Nakamura et al. 2015, Ruggieri et al. 2017)—but not all (e.g. Orsolini et al. 2012)—previous studies. The Pacific sector shows an equivalent barotropic circulation response with positive (anticyclonic) anomalies at lower (SLP, Fig. 3b) and upper levels (Z500, Fig. 3d). Associated with this anticyclonic anomaly, there is a precipitation

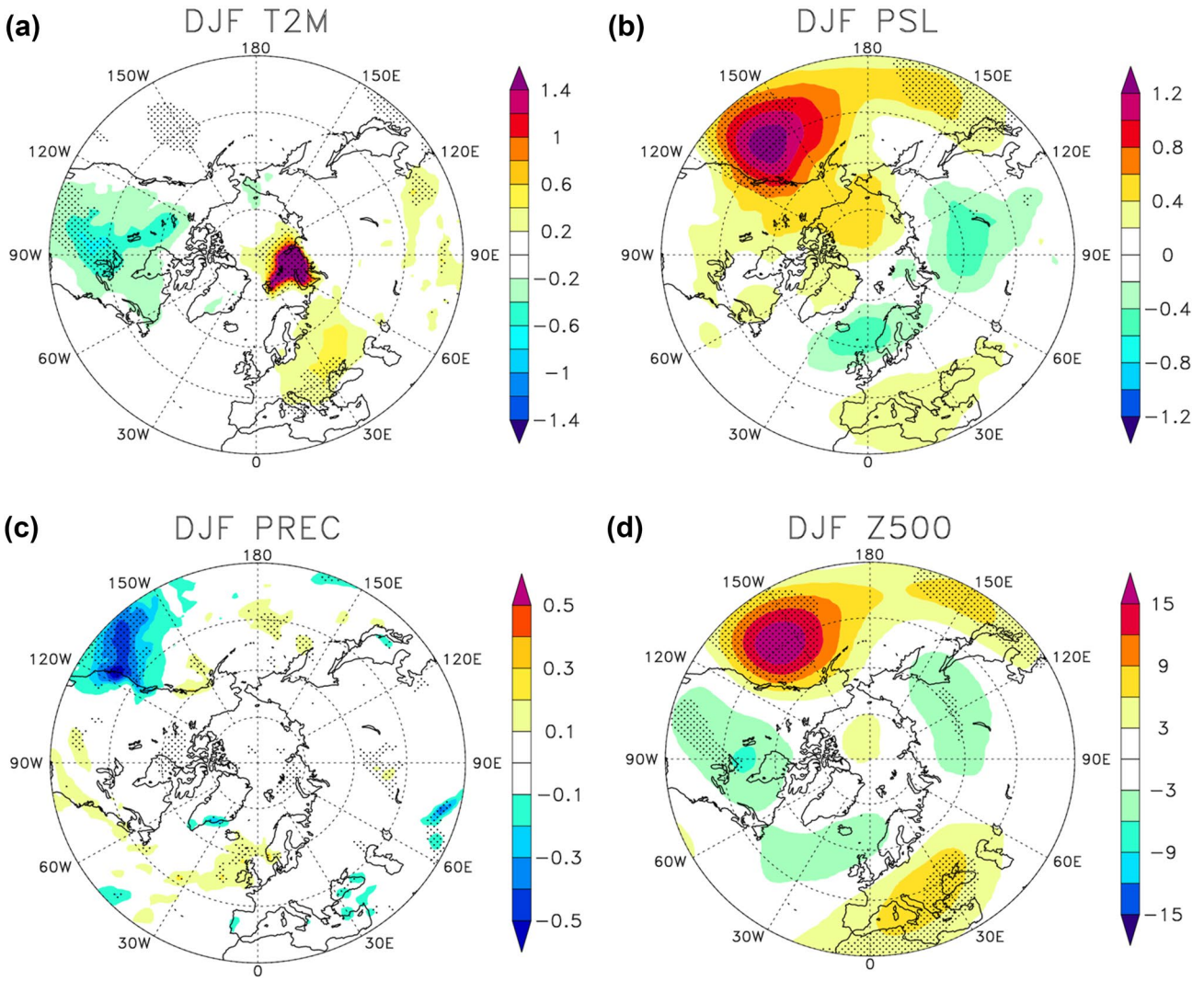

Fig. 3 Winter (DJF) mean surface and large-scale circulation features in response to late autumn sea ice loss. **a** Near-surface (2 m) temperature (°C), **b** mean sea level pressure (hPa), **c** total precipitation (convective + large-scale; mm/day), and **d** geopotential height (m). All fields are defined as the ensemble mean difference between ICEFREE and CTRL. Stippling indicates a statistically different mean between ICEFREE and CTRL to the 95% confidence level

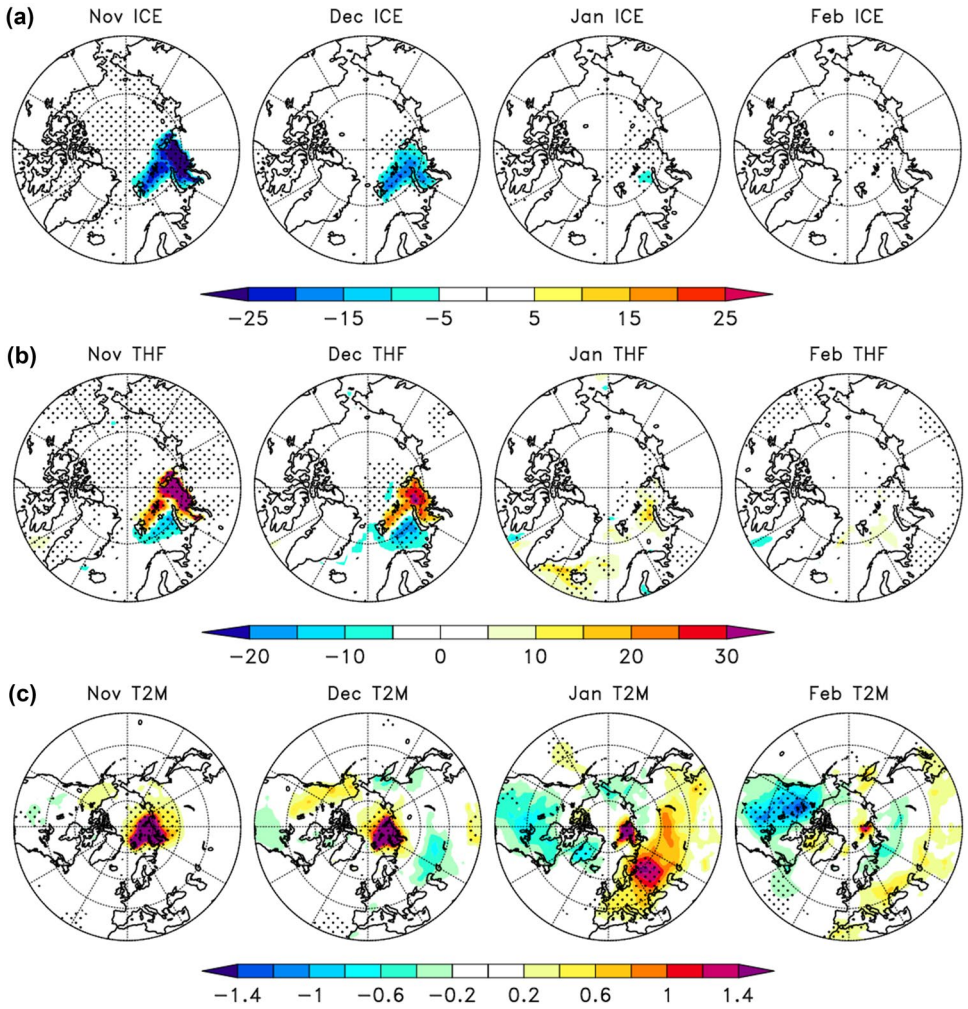

Fig. 4 Transient winter (November-February) surface thermodynamic response to eastern Arctic sea ice loss. Ensemble mean difference (ICEFREE minus CTRL) in **a** sea ice concentration (%), **b** surface turbulent heat fluxes (sensible + latent; W/m^2) and **c** 2 m-temperature (deg C). Stippling indicates a statistically different mean between ICEFREE and CTRL to the 95% confidence level

deficit (dry conditions) over the North American southwest (Fig. 3c). Drought conditions in this area in relation to anticyclonic flow conditions have been a characteristic during recent decades (Wang et al. 2014; Seager et al. 2015), and appear in detrended reanalysis data when contrasting low sea ice years with high sea ice years (Figs. S5–S7). In the following, we will shed light on the role of autumn BKS sea ice perturbation in the transient evolution of this synoptic configuration.

3.2 Seasonal evolution of the thermodynamic and circulation changes

The month-by-month view of the climatic response to the heat flux perturbation in the BKS is depicted in Fig. 4. The sea ice anomaly persists into December, a month after the sea ice restoring in the BKS ends (Fig. 4a). The reduction in sea ice cover (i.e. mainly due to the prevention of sea ice formation) results in strong upward turbulent heat flux anomalies (sensible plus latent heat) from the ocean to the atmosphere in the northern Barents and over the entire Kara Sea (Fig. 4b). Negative heat flux anomalies are found south of the sea ice removal, in regions that, in CTRL, are adjacent to the ice edge where heat loss from the ocean to the atmosphere is largest. In contrast to sea ice anomalies and related surface heat flux changes, near-surface air temperature anomalies spread far beyond regions of the imposed forcing and persist until late winter (Fig. 4c).

While surface changes appear immediately (Fig. 4), most of the large-scale circulation anomalies appear with a delay of 1–2 months (Fig. 5). As a result of ascending air motion, a small localized cyclonic anomaly develops directly over the heating area in November (Fig. 5a) similar to the findings of early classical studies (e.g. Hoskins and Karoly 1981; Honda et al. 2009). However, sea level pressure and geopotential height anomalies are developed across the northern midlatitudes only by December (Fig. 5a,b). Over the Atlantic, we see a strengthening of the Icelandic pressure low and Azores high in January. Corresponding low-level westerly flow (Fig. 5c) in the Atlantic sector is extended downstream and intensified according to the sharper meridional pressure gradient. Together with anomalies in total precipitation,

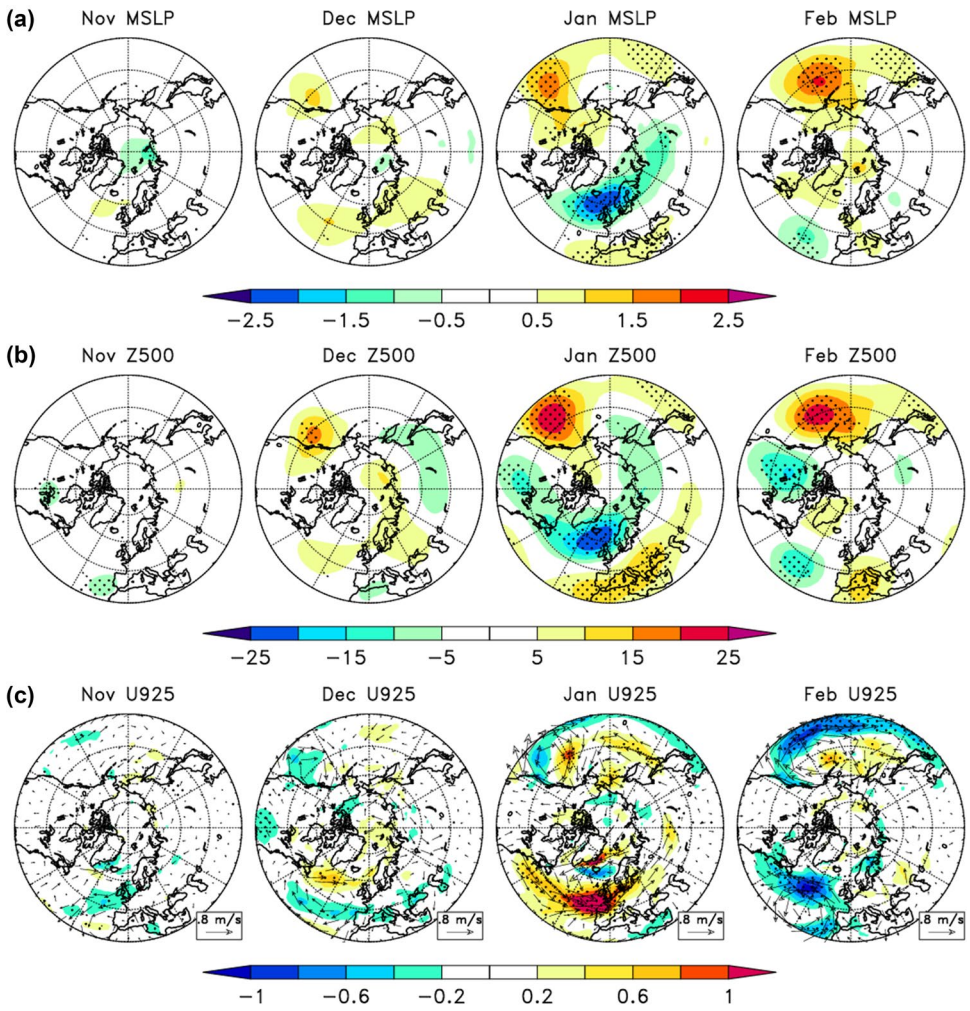

Fig. 5 Transient winter (November-February) circulation response to eastern Arctic sea ice loss. Ensemble mean difference (ICEFREE minus CTRL) in **a** mean sea level pressure (hPa), **b** geopotential height at 500 hPa (m), **c** zonal wind speed at 925 hPa (m/s), overlaid with 925 hPa wind vectors. Stippling indicates a statistically different mean between ICEFREE and CTRL to the 95% confidence level

these features are reminiscent of an NAO + circulation pattern (Fig. S2). However, this NAO + type of response is statistically significant during January only.

In the Pacific sector, a robust and persistent anticyclonic circulation anomaly develops at both lower (Fig. 5a) and upper levels (Fig. 5b), lasting over the entire winter season (Dec–Feb). These features are dominant in the winter mean circulation response (Fig. 3). This geopotential height anomaly diverts westerly flow to the northeast, giving rise to cold anomalies over the North American continent (Figs. 4c, 5c). The Pacific circulation response is addressed in more detail in the next section.

3.3 Pacific circulation response

In order to better understand the synoptic situation in the North Pacific, we focus on the Pacific circulation response during January, when the anomalies are largest. The North Pacific anticyclonic geopotential height anomaly (Fig. 6a) drives a decline in total (convective plus large-scale) precipitation over the American southwest (Fig. 6b), by diverting the wet westerly air masses northward, and thereby leaving the southwest coast of North America anomalously dry. Both the anomalous ridge and the precipitation deficit have been related to Arctic sea ice loss in decadal coupled climate model simulations (Cvijanovic et al. 2017; Sewall and Sloan 2004; Sewall 2005). Cvijanovic et al. (2017) suggested that changes in the North Pacific circulation are a result of reorganization of tropical Pacific convection—analogous to the teleconnection at work during the different phases of the ENSO cycle (e.g. Trenberth et al. 1998).

Similar to the findings of Cvijanovic et al. (2017), in our simulations we find altered tropical Pacific convection. Positive outgoing longwave radiation (OLR) anomalies in the western tropical Pacific (about 160–180 E, 10 N; Fig. 6d) are indicative of weakened deep convection in this area, due to more radiation being emitted at lower altitudes with a warmer cloud top (not shown). Earlier studies, such as Trenberth et al. (1998), have emphasized the importance of anomalies in the divergent flow component in the upper troposphere for stationary Rossby wave generation. The tropical Pacific OLR increase and associated reduced

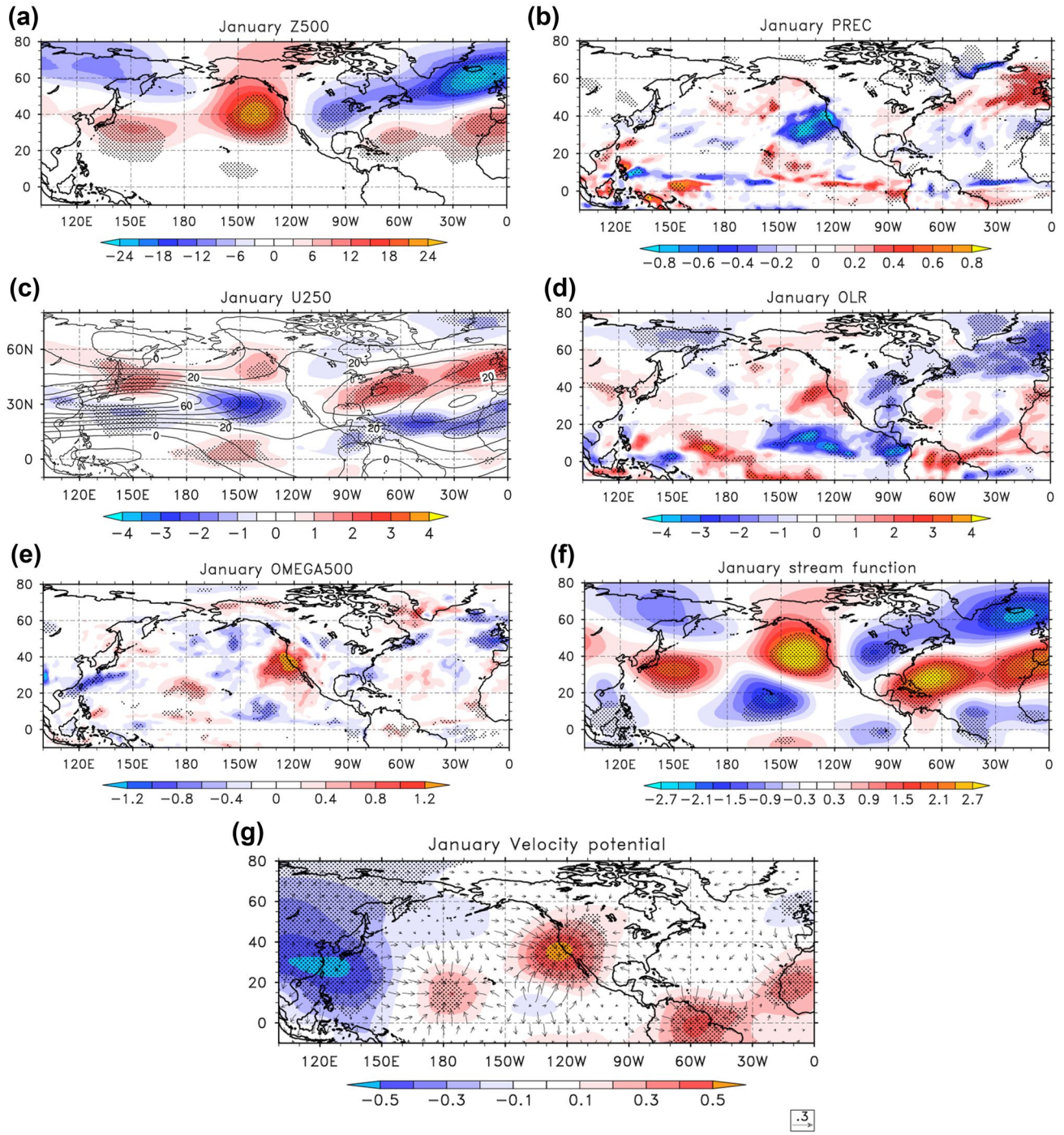

Fig. 6 Mid-winter (January) Pacific circulation response to late autumn Arctic sea ice loss. Ensemble mean difference (ICEFREE minus CTRL) in **a** geopotential height at the 500 hPa level (Z500; m), **b** total precipitation (large-scale + convective; mm/day), **c** zonal winds at 250 hPa (m/s), **d** outgoing longwave radiation (OLR) at the top-of-the-atmosphere (TOA) in W/m^2, **e** vertical velocity at 500 hPa (hPa/s) and **f** stream function (*10^6 m^2/s) computed from the horizontal wind components (u,v) at 250 hPa. g) Velocity potential (*10^6 m^2/s; colours) and divergent winds components (vectors) computed from horizontal wind components (u,v) at 250 hPa. Stippling indicates a statistically different mean between ICEFREE and CTRL to the 95% confidence level

deep convection seen in our simulations are consistent with reduced upper-level divergence (Fig. 6g), that drives a Rossby wave train to the extratropical North Pacific (note that anomalies in upper-level divergence/velocity potential and OLR are slightly offset due to the fact that the velocity potential reflects a large-scale field, while changes in convective activity (OLR) are on a local scale).

The Rossby wave train is indicated by a cyclonic circulation cell just northeast of the positive OLR anomaly, followed by an anticyclonic circulation cell in the northern extratropical Pacific, at the same location as the geopotential height anomaly (Fig. 6a). This class of Rossby waves takes about a month to get established, and the waves travel along great circles (Wallace and Gutzler 1981). The anticyclonic flow anomaly at 250 hPa is thus an upper-level manifestation of the 500 hPa geopotential height anomaly (Fig. 6a), pointing to equivalent barotropic circulation anomalies.

Thus, the development of the North Pacific anticyclonic circulation anomaly may be understood in the light of reduced convective activity in the western tropical Pacific, even though the dominant role of this mechanism is not unequivocal, and other interpretations are possible.

3.4 Extratropical forcing of tropical convection changes

This section explores ways in which Arctic forcing may influence the tropical Pacific on the seasonal timescale of interest. From an energetics perspective, the tropical OLR changes seen in our simulations may be a start of an adjustment to the energy surplus at high latitudes originating from the imposed heating perturbation in November. Cvijanovic et al. (2017) noted an increase in top-of-the-atmosphere (TOA) radiation to space in the tropical Pacific between 20° S and 20° N and an associated reduction in the northward atmospheric heat transport. Our 6-month long simulations are, however, far from equilibrium, and energy budget considerations are less relevant at these time scales.

Some clues emerge from considering the surface responses in the tropical Pacific. In the western tropical Pacific, we see cold SST anomalies collocated with strengthened near-surface easterly winds, while in the eastern tropical Pacific, we see warm SST anomalies collocated with weakened easterlies (Fig. 7, Fig. 8 a,b). Where the near-surface winds are stronger (weaker), there are increased (decreased) latent heat fluxes from the ocean to the atmosphere (Fig. 8c). Locally, these signals are consistent with the so-called "wind-evaporation-sea surface temperature" (WES) feedback highlighted in previous studies as a mechanism for communication from the extratropics to the tropics (Chiang and Bitz 2005; Mahajan et al. 2011; Cvijanovic and Chiang 2013). Similar to the findings of these studies, the locations of positive OLR anomalies (associated with large-scale convective changes) are collocated with the areas of cold SST anomalies and strengthened easterly winds. It is however important to note that the tropical Pacific response seen in our simulations is different in shape (i.e., not as zonally symmetric) compared to the ones reported above. This is most likely a consequence of the different timescales

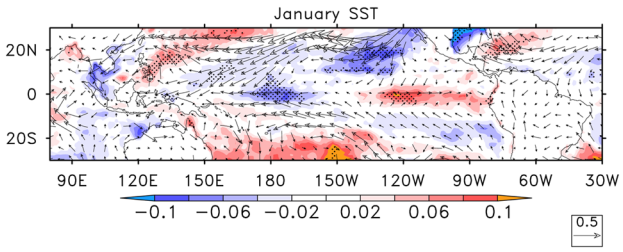

Fig. 7 Mid-winter (January) tropical Pacific SST and near-surface wind (925 hPa; arrows) anomalies in response to November Arctic sea ice loss in the BKS. Shading indicates the ensemble mean difference between ICEFREE and CTRL. Stippling indicates statistically different mean between ICEFREE and CTRL to the 95% confidence level

and geometry of the high-latitude forcing considered in our study.

Another feature of the Pacific circulation changes in response to autumn Arctic sea ice loss is a retraction and slight poleward shift of the Pacific jet stream in the area of maximum upper westerly flow (at ~ 150°E ; see contours in Fig. 6c). Such changes are associated with well-known patterns of North Pacific variability affecting the storm track and precipitation over North America (Athanasiadis et al. 2010; Wettstein and Wallace 2010). The Pacific jet is driven both by tropical heating and eddy fluxes (Li et al. 2012), which means that it can also communicate changes from the extratropics to the tropics. Idealized experiments show that changes in midlatitude eddy activity can affect the Hadley cell via feedbacks between eddy fluxes and the mean flow (Schneider and Bordoni 2008; Mbengue and Woollings 2019). Our imposed Arctic heating weakens the meridional surface temperature gradient (Fig. S8), which reduces surface baroclinicity and, presumably, the eddy-driven component of the jet. Detailed evidence for eddy-driven changes are not deducible from the current analysis, however.

Different processes described here, as suggested in earlier studies, are not mutually exclusive, but likely operate on different timescales. The question of dominance of one of these pathways over another and the timescale at which this occurs, is however, beyond the scope of our study.

4 Discussion and conclusion

The wintertime Northern Hemisphere atmospheric circulation response to late autumn eastern Arctic sea ice reduction was assessed in a set of seasonal predictions. The circulation response in the Euro-Atlantic sector is ephemeral (resembling the NAO + phase), lasting only through the month of January, and thus corroborates previous findings of an intermittent and non-stationary NAO response to eastern Arctic sea ice loss as seen in observations (Siew

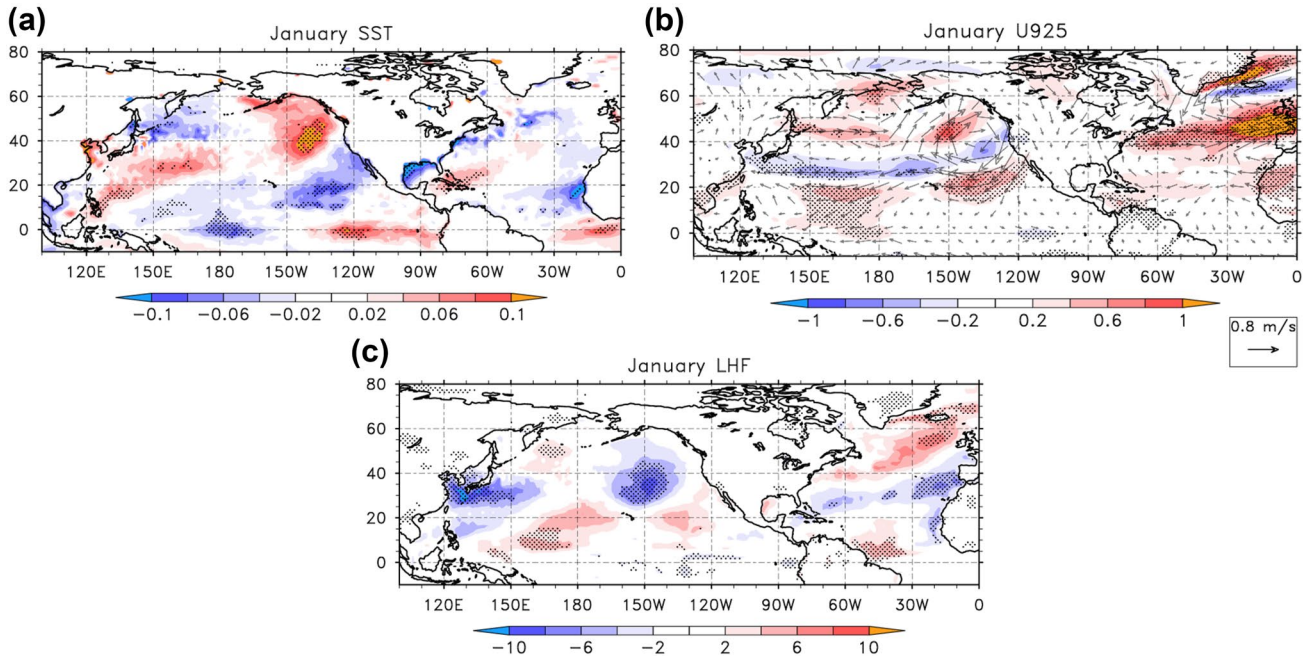

Fig. 8 Mid-winter (January) Pacific surface response to late autumn Arctic sea ice loss. Ensemble mean difference (ICEFREE minus CTRL) in **a** sea surface temperatures (SST, °C) and **b** low-level zonal wind speed computed from zonal (u) and meridional (v) wind components at 925 hPa (colors) and direction and magnitude of these low-level winds (arrows), and **c)** surface latent heat fluxes (W/m^2). Stippling indicates statistically different mean between ICEFREE and CTRL to the 95% confidence level

et al. 2020; Kolstad and Screen 2019). On the other hand, a robust and marked anticyclonic flow anomaly at upper and lower levels develops in the northeast Pacific sector (December–February). This anticyclonic anomaly leads to drying in the North American southwest, a result noted in previous studies on the (multi-)decadal time scale. The response is tied to dominant well-known patterns of North Pacific variability affecting precipitation over North America, and finds new applications here in the seasonal prediction framework. The mechanism suggested in this study involves a Pacific "Flip-Flop" in which midlatitude eddy activity weakens the Hadley cell, and thus convective activity in the western tropical Pacific, even though other interpretations are possible. Anomalies in the tropical upper-level divergence where convection is weakened trigger a Rossby wave train back to extratropical latitudes, resulting in the described anticyclonic flow anomaly. This mechanism is suggested for the first time on the seasonal time scale, and for the first time in response to sea ice loss constrained to the eastern Arctic basin. Our anomalies hold true even when removing strong El Niño and La Niña years, indicating that the mechanism identified is a robust feature independent of ENSO (Figs. S3, S4).

Previous studies demonstrated a delayed NAO-like circulation signal in the Euro-Atlantic sector due to anomalous upward propagating planetary wave activity and a subsequent weakening of the stratospheric polar vortex, following autumn Arctic sea ice anomalies. Whether anomalous stratospheric activity plays a role in the winter circulation response seen in our simulations will be subject of future research.

A prominent anticyclonic circulation anomaly in response to Arctic sea ice loss is also the result of AGCM studies coupled to a slab ocean, hence omitting deep ocean dynamics (Cvijanovic et al. 2017). This points to the fact that qualitatively the same circulation signal in the North Pacific as identified here can be obtained without the contribution of the ocean dynamics, which latter was postulated to shape significantly the Pacific extratropical circulation response (e.g. England et al. 2020; Tomas et al. 2016; Wang et al. 2018).

In contrast to our findings, a series of earlier studies observe a strengthening of the Aleutian low in response to Arctic sea ice loss (Oudar et al. 2017; McCusker et al. 2017; Blackport and Kushner 2017; Deser et al. 2015; Tomas et al. 2016). This is consistent with the fact that such studies run their simulations on a century-long timescale, so that effects related to changes in the Atlantic Meridional Overturning Circulation (AMOC) become apparent and relevant. In fact, a slow-down of the AMOC is evident in simulations of projected Arctic sea ice loss and greenhouse gas (GHG) forcing, having identified a deepening of the Aleutian low (combined and separately; McCusker et al. 2017; Oudar et al. 2017).

Our study adopts a non energy-conserving heat flux adjustment to the surface ocean non-solar heat fluxes. One of the questions discussed in the literature is to what extent the methodology to perturb the sea ice cover may influence aspects of the circulation response to Arctic sea ice loss (e.g. Sun et al. 2020). Previous studies employing energy-conserving sea ice perturbation methods report similar circulation changes in the North Pacific sector (e.g. Cvijanovic et al. 2015; Simon et al. 2021), which lends credibility to our results and methodology. However, we do not believe that the methodology of sea ice perturbation is dominant in shaping the circulation response on the timescales considered in this study.

In conclusion, while there are other factors potentially affecting precipitation over the North American southwest (California in particular), such as those related to the different phases of the ENSO cycle, the presented analysis suggests that Arctic sea ice loss can be regarded as one possible driver and as source of predictability for winter drought conditions over the North American southwest.

Supplementary Information The online version contains supplementary material available at https://doi.org/10.1007/s00382-021-05830-9.

Acknowledgements This study was supported by the Blue-Action project (European Union's Horizon 2020 research and innovation programme, Grant 727852). I.C. was supported by Generalitat de Catalunya (Secretaria d'Universitats i Recerca del Departament d'Empresa i Coneixement) through Beatriu de Pinós programme. C.L. acknowledges support from the Research Council of Norway (DynAMiTe grant 255027). The figures were produced with the NCAR Command Language Software (10.5065/D6WD3XH5).

Authors contributions AS performed all the simulations, produced all the plots and contributed the major part of this manuscript. PA provided guidance in the experimental design, the analysis part and the overall interpretation of the results. PR provided guidance to the literature review and helped resolving some technical issues in successfully running the simulations. CL helped in the dynamical interpretation of the results and provided additional insights regarding the extratropical-tropical connection in this study. IC provided useful guidance in putting the results into context with the existing literature. SG provided guidance on all aspects of the manuscript.

Funding This study was supported by the Blue-Action project (European Union's Horizon 2020 research and innovation programme, Grant 727852.

Availability of data and material Upon request.

Code availability Upon request.

Declarations

Conflicts of interest/competing interest The authors declares that they have no competing interest.

References

Athanasiadis PJ, Wallace JM, Wettstein JJ (2010) Patterns of wintertime jet stream variability and their relation to the storm tracks. J Atmos Sci 67(5):1361–1381

Blackport R, Kushner PJ (2017) Isolating the atmospheric circulation response to Arctic sea ice loss in the coupled climate system. J Clim 30(6):2163–2185

Blackport R, Screen JA, van der Wiel K, Bintanja R (2019) Minimal influence of reduced Arctic sea ice on coincident cold winters in mid-latitudes. Nat Clim Chang 9(9):697–704

Boer GJ, Smith DM, Cassou C, Doblas-Reyes F, Danabasoglu G, Kirtman B, Kushnir Y, Kimoto M, Meehl GA, Msadek R, Mueller WA (2016) The decadal climate prediction project (DCPP) contribution to CMIP6. GeosciModel Dev (Online) 9(10):3751–3777

Chiang JC, Bitz CM (2005) Influence of high latitude ice cover on the marine Intertropical Convergence Zone. Clim Dyn 25(5):477–496

Cvijanovic I, Chiang JC (2013) Global energy budget changes to high latitude North Atlantic cooling and the tropical ITCZ response. Clim Dyn 40(5–6):1435–1452

Cvijanovic I, Caldeira K, MacMartin DG (2015) Impacts of ocean albedo alteration on Arctic sea ice restoration and Northern Hemisphere climate. Environ Res Lett 10(4):044020

Cvijanovic I, Santer BD, Bonfils C, Lucas DD, Chiang JC, Zimmerman S (2017) Future loss of Arctic sea-ice cover could drive a substantial decrease in California's rainfall. Nat Commun 8(1):1–10

Deser G, Magnusdottir RS, Phillips AS (2004) The effects of North Atlantic SST and sea-ice anomalies on the winter circulation in CCM3. Part II: Direct and indirect components of the response. J Clim 17:877–889

Deser C, Tomas RA, Peng S (2007) The transient atmospheric circulation response to North Atlantic SST and sea ice anomalies. J Clim 20(18):4751–4767

Deser C, Tomas R, Alexander M, Lawrence D (2010) The seasonal atmospheric response to projected Arctic sea ice loss in the late 21st century. J Clim 23:333–351. https://doi.org/10.1175/2009JCLI3053.1

Deser C, Tomas RA, Sun L (2015) The role of ocean–atmosphere coupling in the zonal-mean atmospheric response to Arctic sea ice loss. J Clim 28(6):2168–2186

England MR, Polvani LM, Sun L, Deser C (2020) Tropical climate responses to projected Arctic and Antarctic sea-ice loss. Nat Geosci 13(4):275–281

García-Serrano J, Frankignoul C, Gastineau G, de La Càmara A (2015) On the predictability of the winter Euro-Atlantic climate: lagged influence of autumn Arctic sea ice. J Clim 28(13):5195–5216

Honda M, Inoue J, Yamane S (2009) Influence of low Arctic sea-ice minima on anomalously cold Eurasian winters. Geophys Res Lett. https://doi.org/10.1029/2008GL037079

Hoskins BJ, Karoly DJ (1981) The steady linear response of a spherical atmosphere to thermal and orographic forcing. J Atmos Sci 38(6):1179–1196

Kim BM, Son SW, Min SK, Jeong JH, Kim SJ, Zhang X, Shim T, Yoon JH (2014) Weakening of the stratospheric polar vortex by Arctic sea-ice loss. Nat Commun 5(1):1–8

Koenigk T, Caian M, Nikulin G, Schimanke S (2016) Regional Arctic sea ice variations as predictor for winter climate conditions. Clim Dyn 46(1–2):317–337

Kolstad EW, Screen JA (2019) Nonstationary relationship between autumn Arctic sea ice and the winter North Atlantic oscillation. Geophys Res Lett 46(13):7583–7591

Kug JS, Jeong JH, Jang YS, Kim BM, Folland CK, Min SK, Son SW (2015) Two distinct influences of Arctic warming on cold winters over North America and East Asia. Nat Geosci 8(10):759–762

Liu J, Curry JA, Wang H, Song M, Horton RM (2012) Impact of declining Arctic sea ice on winter snowfall. Proc Natl Acad Sci 109(11):4074–4079

Mahajan S, Saravanan R, Chang P (2011) The role of the wind–evaporation–sea surface temperature (WES) feedback as a thermodynamic pathway for the equatorward propagation of high-latitude sea ice–induced cold anomalies. J Clim 24(5):1350–1361

Mbengue CO, Woollings T (2019) The Eddy-driven jet and storm-track responses to boundary layer drag: insights from an idealized dry GCM study. J Atmos Sci 76(4):1055–1076

McCusker KE, Fyfe JC, Sigmond M (2016) Twenty-five winters of unexpected Eurasian cooling unlikely due to Arctic sea-ice loss. Nat Geosci 9(11):838–842

McCusker KE, Kushner PJ, Fyfe JC, Sigmond M, Kharin VV, Bitz CM (2017) Remarkable separability of circulation response to Arctic sea ice loss and greenhouse gas forcing. Geophys Res Lett 44(15):7955–7964

Meredith M, Sommerkorn M, Cassotta S, Derksen C, Ekaykin A, Hollowed A, Kofinas G, Mackintosh A, Melbourne-Thomas J, Muelbert MMC, Ottersen G, Pritchard H, Schuur EAG (2019) Polar regions. In: Pörtner H-O, Roberts DC, Masson-Delmotte V, Zhai P, Tignor M, Poloczanska E, Mintenbeck K, Alegría A, Nicolai M, Okem A, Petzold J, Rama B, Weyer NM (eds) IPCC Special Report on the Ocean and Cryosphere in a Changing Climate. [Pörtner H-O, Roberts DC, Masson-Delmotte V, Zhai P, Tignor M, Poloczanska E, Mintenbeck K, Alegría A, Nicolai M, Okem A, Petzold J, Rama B, Weyer NM (eds)]. In press

Nakamura T, Yamazaki K, Iwamoto K, Honda M, Miyoshi Y, Ogawa Y, Ukita J (2015) A negative phase shift of the winter AO/NAO due to the recent Arctic sea-ice reduction in late autumn. J Geophys Res Atmos 120(8):3209–3227

Onarheim IH, Eldevik T, Smedsrud LH, Stroeve JC (2018) Seasonal and regional manifestation of Arctic sea ice loss. J Clim 31(12):4917–4932

Orsolini YJ, Senan R, Benestad RE, Melsom A (2012) Autumn atmospheric response to the 2007 low Arctic sea ice extent in coupled ocean–atmosphere hindcasts. Clim Dyn 38(11–12):2437–2448

Oudar T, Sanchez-Gomez E, Chauvin F, Cattiaux J, Terray L, Cassou C (2017) Respective roles of direct GHG radiative forcing and induced Arctic sea ice loss on the Northern Hemisphere atmospheric circulation. Clim Dyn 49(11–12):3693–3713

Peings Y, Magnusdottir G (2014) Response of the wintertime Northern Hemisphere atmospheric circulation to current and projected Arctic sea ice decline: a numerical study with CAM5. J Clim 27(1):244–264

Ruggieri P, Kucharski F, Buizza R, Ambaum MHP (2017) The transient atmospheric response to a reduction of sea-ice cover in the Barents and Kara Seas. Q J R Meteorol Soc 143(704):1632–1640

Sanna A, Borrelli A, Athanasiadis P, Materia S, Storto A, Tibaldi S, Gualdi S (2017) CMCC-SPS3: the CMCC Seasonal Prediction System 3. Centro Euro-Mediterraneo sui Cambiamenti Climatici. CMCC Tech. Rep. RP0285, p 61

Scaife AA, Arribas A, Blockley E, Brookshaw A, Clark RT, Dunstone N, Eade R, Fereday D, Folland CK, Gordon M, Hermanson L, Knight JR, Lea DJ, MacLachlan C, Maidens A, Martin M, Peterson AK, Smith D, Vellinga M, Wallace E, Waters J, Williams A (2014) Skillful long-range prediction of European and North American winters. Geophys Res Lett 41:2514–2519. https://doi.org/10.1002/2014GL059637

Schneider T, Bordoni S (2008) Eddy-mediated regime transitions in the seasonal cycle of a Hadley circulation and implications for monsoon dynamics. J Atmos Sci 65(3):915–934

Screen JA (2017) Simulated atmospheric response to regional and pan-Arctic sea ice loss. J Clim 30(11):3945–3962

Screen JA, Simmonds I (2013) Exploring links between Arctic amplification and mid-latitude weather. Geophys Res Lett 40(5):959–964

Screen JA, Simmonds I, Deser C, Tomas R (2013) The atmospheric response to three decades of observed Arctic sea ice loss. J clim 26(4):1230–1248

Screen JA, Deser C, Smith DM, Zhang X, Blackport R, Kushner PJ, Oudar T, McCusker KE, Sun L (2018) Consistency and discrepancy in the atmospheric response to Arctic sea-ice loss across climate models. Nat Geosci 11(3):155–163

Seager RH, Wang M, Lyon SSH, Kumar BA, Henderson JNN (2015) Causes and predictability of the 2011–14 California drought. http://cpo.noaa.gov/MAPP/californiadroughtreport. Accessed 10 Oct 2020

Seierstad IA, Bader J (2009) Impact of a projected future Arctic sea ice reduction on extratropical storminess and the NAO. Clim Dyn 33(7–8):937

Semmler T, Stulic L, Jung T, Tilinina N, Campos C, Gulev S, Koracin D (2016) Seasonal atmospheric responses to reduced arctic sea ice in an ensemble of coupled model simulations. J Clim 29(16):5893–5913

Sewall JO (2005) Precipitation shifts over western North America as a result of declining Arctic sea ice cover: The coupled system response. Earth Interact 9(26):1–23

Sewall JO, Sloan LC (2004) Disappearing Arctic sea ice reduces available water in the American west. Geophys Res Lett 31:L06209

Siew PYF, Li C, Sobolowski SP, King MP (2020) Intermittency of Arctic–mid-latitude teleconnections: stratospheric pathway between autumn sea ice and the winter North Atlantic Oscillation. Weather Clim Dyn 1(1):261–275

Simon A, Gastineau G, Frankignoul C, Rousset C, Codron F (2021) Transient climate response to Arctic sea-ice loss with two ice-constraining methods. J Clim 34(9):1–50

Singarayer JS, Bamber JL, Valdes PJ (2006) Twenty-first-century climate impacts from a declining Arctic sea ice cover. J Clim 19(7):1109–1125

Sun L, Deser C, Tomas RA, Alexander M (2020) Global coupled climate response to polar sea ice loss: evaluating the effectiveness of different ice-constraining approaches. Geophys Res Lett 47(3):e2019GL085788

Tomas RA, Deser C, Sun L (2016) The role of ocean heat transport in the global climate response to projected Arctic sea ice loss. J Clim 29(19):6841–6859

Trenberth KE, Branstator GW, Karoly D, Kumar A, Lau NC, Ropelewski C (1998) Progress during TOGA in understanding and modeling global teleconnections associated with tropical sea surface temperatures. J Geophys Res Oceans 103(C7):14291–14324

Wallace JM, Gutzler DS (1981) Teleconnections in the geopotential height field during the Northern Hemisphere winter. Mon Weather Rev 109:784–812

Wang SY, Hipps L, Gillies RR, Yoon JH (2014) Probable causes of the abnormal ridge accompanying the 2013–2014 California drought: ENSO precursor and anthropogenic warming footprint. Geophys Res Lett 41(9):3220–3226

Wang K, Deser C, Sun L, Tomas RA (2018) Fast response of the tropics to an abrupt loss of Arctic sea ice via ocean dynamics. Geophys Res Lett 45(9):4264–4272

Wettstein JJ, Wallace JM (2010) Observed patterns of month-to-month storm-track variability and their relationship to the background flow. J Atmos Sci 67(5):1420–1437

Wilks DS (2011) Statistical methods in the atmospheric sciences, vol 100. Academic Press

Yang XY, Yuan X, Ting M (2016) Dynamical link between the Barents-Kara sea ice and the Arctic Oscillation. J Clim 29(14):5103–5122